Effect of growth temperature on the microstructure and properties of epitaxial MoS₂ monolayers grown by metalorganic chemical vapor deposition FREE

Special Collection: 55 Years of Metalorganic Chemical Vapor Deposition (MOCVD)

Chen Chen ; Nicholas Trainor ; Shalini Kumari ; Henrik Myja ; Tilmar Kümmell; Zhiyu Zhang ; Yuxi Zhang ; Anuj Bisht; Muhtasim UI Karim Sadaf ; Najam U. Sakib ; Ying Han ; Thomas V. Mc Knight ; Andrew R. Graves ; Meghan E. Leger ; Nicholas D. Redwing; Myeongok Kim ; Dorota Anna Kowalczyk ; Gerd Bacher ; Nasim Alem ; Yang Yang ; Saptarshi Das ; Joan M. Redwing



J. Vac. Sci. Technol. A 42, 022201 (2024) https://doi.org/10.1116/6.0003296





CrossMark





Effect of growth temperature on the microstructure and properties of epitaxial MoS₂ monolayers grown by metalorganic chemical vapor deposition

Cite as: J. Vac. Sci. Technol. A 42, 022201 (2024); doi: 10.1116/6.0003296 Submitted: 10 November 2023 · Accepted: 10 January 2024 · Published Online: 2 February 2024







Chen Chen, 1 D Nicholas Trainor, 12 D Shalini Kumari, 12 D Henrik Myja, 3 D Tilmar Kümmell, 3 Zhiyu Zhang, 4 D Yuxi Zhang,² 🕩 Anuj Bisht,^{1,5} Muhtasim Ul Karim Sadaf,⁴ 🕩 Najam U. Sakib,⁴ 🕩 Ying Han,⁴ 🕩 Thomas V. Mc Knight,^{1,2} 🕩 Andrew R. Graves, 1 📵 Meghan E. Leger, 1.2 📵 Nicholas D. Redwing, 2 📵 Myeongok Kim, 6 📵 Dorota Anna Kowalczyk, 7 📵

AFFILIATIONS

- ¹2D Crystal Consortium—Materials Innovation Platform, Materials Research Institute, The Pennsylvania State University, University Park, Pennsylvania 16802
- 2 Department of Materials Science and Engineering, The Pennsylvania State University, University Park, Pennsylvania 16802
- ³Werkstoffe der Elektrotechnik and CENIDE, University of Duisburg-Essen, Duisburg 47057, Germany
- ⁴Department of Engineering Science and Mechanics, The Pennsylvania State University, University Park, Pennsylvania 16802
- ⁵Department of Metallurgical and Materials Engineering, Indian Institute of Technology Kharagpur, Kharagpur 721302, India
- ⁶School of Engineering, The University of Tokyo, Tokyo 113-8656, Japan, Japan
- Department of Solid-State Physics, Faculty of Physics and Applied Informatics, University of Lodz, Pomorska 149/153, Lodz 90-236, Poland
- ⁸Department of Electrical Engineering and Computer Science, The Pennsylvania State University, University Park, Pennsylvania 16802

Note: This paper is part of the Special Topic Collection —55 Years of Metalorganic Chemical Vapor Deposition (MOCVD). a)Electronic mail: jmr31@psu.edu

ABSTRACT

Metalorganic chemical vapor deposition (MOCVD) is a promising technique for wafer-scale synthesis of MoS₂ monolayers for 2D fieldeffect transistors (2D-FETs) and related devices. Epitaxial growth of MoS2 on sapphire provides films that are crystallographically well-oriented but typically contain low-angle grain boundaries (e.g., mirror twins), voids, and other defects depending on growth conditions and substrate characteristics. In this study, we investigate microstructure, optical properties, and field-effect characteristics of wafer-scale MoS₂ monolayers grown by MOCVD on c-plane sapphire over a narrow window of growth temperatures (900-1000 °C). The density of low-angle grain boundaries in the MoS₂ monolayer was found to decrease dramatically from 50% areal coverage for films grown at 900 °C to 5% at 1000 °C. This decrease in low-angle grain boundary density is correlated with an increase in the room-temperature photoluminescence intensity of A excitons and a decrease in the full-width-half maximum (FWHM) of the Raman A_{1g} peak, which are typically indicative of a general reduction in defects in MoS2. However, the best transport properties (e.g., mean field-effect mobility m_{FE} = 17.3 cm²/V s) were obtained in MoS₂ monolayers grown at an intermediate temperature of 950 °C. It was found that as the growth temperature increased, small regions bound by high-angle boundaries begin to appear within the monolayer and increase in areal coverage, from ~2% at 900 °C to ~5% at 950 °C to ~10% at 1000 °C. The growth temperature of 950 °C, therefore, provides an intermediate condition where the combined effects of low-angle and high-angle boundaries are minimized. The results of this study provide guidance on MOCVD growth and characterization that can be used to further optimize the performance of MoS₂ 2D-FETs.

Published under an exclusive license by the AVS. https://doi.org/10.1116/6.0003296



I. INTRODUCTION

Monolayer and few-layer semiconducting transition metal dichalcogenides (TMDs), exemplified by materials like MoS₂, have garnered increasing interest in the realm of 2D field-effect transistors (2D-FETs) for next-generation gate-all-around nanosheet devices and heterogeneous integration with silicon complementary metal-oxidesemiconductor (Si CMOS) technology. 1,2 This burgeoning enthusiasm for TMDs is grounded in their ultrathin body nature, which may enable high-density stacked nanosheets beyond that achievable with silicon as well as low-power electronics needed for edge computing and neuromorphic devices. However, realization of high-performance 2D-FETs requires advances in TMD synthesis to provide high-quality monolayer and few-layer films that can be readily integrated into devices via either direct growth or layer transfer methods.

Among the various methods available for TMD synthesis, metalorganic chemical vapor deposition (MOCVD) has emerged as a promising scalable technique for achieving wafer-scale films via either direct growth of polycrystalline films on amorphous substrates such as oxidized SiO₂/Si substrates at reduced temperature (<600 °C)^{3,4} or high-temperature epitaxy on sapphire.5-7 Epitaxial growth of TMDs on sapphire is a particularly promising approach as it enables control of TMD domain orientation, thereby reducing the density of high-angle grain boundaries.⁸⁻¹¹ While epitaxial growth allows for the creation of large-area, well-aligned TMD films, the domain coalescence process, responsible for forming wafer-scale epitaxial TMD monolayers, often gives rise to various defects. These defects include line defects such as mirror twins (also called inversion domain boundaries) and translational boundaries 12,13 as well as point defects such as chalcogen vacancies and impurities.¹⁴ Understanding the nature and impact of these defects is crucial for advancing the field of TMD-based 2D-FETs toward practical applications.

Despite the growing interest in TMDs for 2D-FETs, attempts to systematically correlate defects in wafer-scale TMD films with device performance have been limited thus far. Therefore, the primary objective of this study is to understand how MOCVD growth conditions, specifically growth temperature, determines the type and quantity of line defects present in wafer-scale epitaxial MoS₂ films to gain insight into their impact on 2D-FET performance. Growth temperature is a crucial parameter in epitaxy since it strongly influences nucleation and surface diffusion processes, which ultimately impact the crystal quality and optical/electrical properties of the MoS₂ monolayers. In this study, we investigate the effects of growth temperature on the properties of MoS2 monolayers grown by MOCVD on c-plane sapphire over a limited temperature range (900-1000 °C) where the films remain epitaxial and growth rate does not vary significantly with temperature. The results reveal marked changes in the type and density of grain boundaries in the MoS₂ monolayers over this temperature window, which are correlated to photoluminescence properties and 2D-FET performance. Our results provide important insights necessary for optimization of the MOCVD process for the synthesis of highquality MoS2 monolayers.

II. EXPERIMENT

MOCVD growth of wafer-scale MoS2 monolayers was carried out in a horizontal cold-wall reactor that includes an induction-

heated rotating SiC-coated graphite susceptor and separate gas inlets for the metal and chalcogen precursors [Fig. S1(a)]. 15 Molybdenum hexacarbonyl [Mo(CO)₆] and hydrogen sulfide (H₂S) were used as precursors in an H₂ carrier gas. C-plane sapphire (2" diameter) with a nominal ±0.2° miscut toward the M-axis was used for all growths. In brief, the MoS₂ monolayer was grown in a single-step process [Fig. S1(b)]²⁸ where the growth temperature was varied as 900, 950, and 1000°C. The flow rate of the molybdenum precursor ranged from 2.3×10^{-3} to 3.5×10^{-3} SCCM, while the H₂S flow rate was maintained at 400 SCCM, resulting in an S/Mo ratio of $\sim 10^5$. Growths were carried out with a moderate reactor pressure of 50 Torr using H2 as the carrier gas, and fully coalesced monolayer MoS₂ was achieved in 30 min across the 2" substrate. Details on the MOCVD growth and characterization are included in the supplementary information.²⁸ In brief, atomic force microscopy (AFM) and field-emission scanning electron microscopy (FESEM) were used to characterize the surface coverage and morphology of the layers. In-plane x-ray diffraction (XRD) was used to assess the crystal quality and epitaxial orientation of the films. Raman spectroscopy was used to evaluate the number of layers and defects/disorder of the films. Transmission electron microscopy (TEM) including selected area electron diffraction (SAED) and dark-field (DF) imaging as well as 4-dimensional scanning transmission electron microscopy (4D-STEM) were used to evaluate the grain structure of the monolayers. Room-temperature photoluminescence (PL) spectroscopy and spatially resolved PL mapping were carried out to assess the optical properties. The MoS₂ monolayers were transferred from sapphire to back-gated field-effect test structures with Ni/Au contacts for the source and drain to characterize the electrical transport properties. Details on the transfer process, FET device fabrication, and electrical characterizations are included in the supplementary information.²

III. RESULTS AND DISCUSSION

A. Surface coverage and morphology of MoS₂ monolayers

The effects of growth temperature on the surface coverage and uniformity of the MoS₂ monolayers across the 2" diameter sapphire substrates were initially investigated over the temperature range from 900 to 1000 °C. This temperature range was chosen as the surface coverage did not vary significantly with temperature, as illustrated in Table S1 and Fig. S4, 28 hence minimizing the effects of growth rate on film properties. The weak temperature dependence suggests that in the range from 900 to 1000 °C, the growth rate of MoS₂ is limited by mass transport of precursors to the surface rather than reaction kinetics similar to that observed previously for MOCVD growth of WSe2.5 It is important to note that similar MoS₂ surface coverage does not imply that the crystallinity and microstructure of the MoS2 monolayers are similar as will be further elucidated in this work.

Visually, the MoS₂ films exhibit a uniform light green color [Fig. 1(a)]. AFM images obtained at the center of the 2" sample [Figs. 1(b)-1(d)] indicate fully coalesced monolayers of MoS₂ that cover the sapphire surface with no visible holes/voids and with additional bilayers (in a form of triangles) and multilayer/ out-of-plane domains (white). Similar morphology is observed for

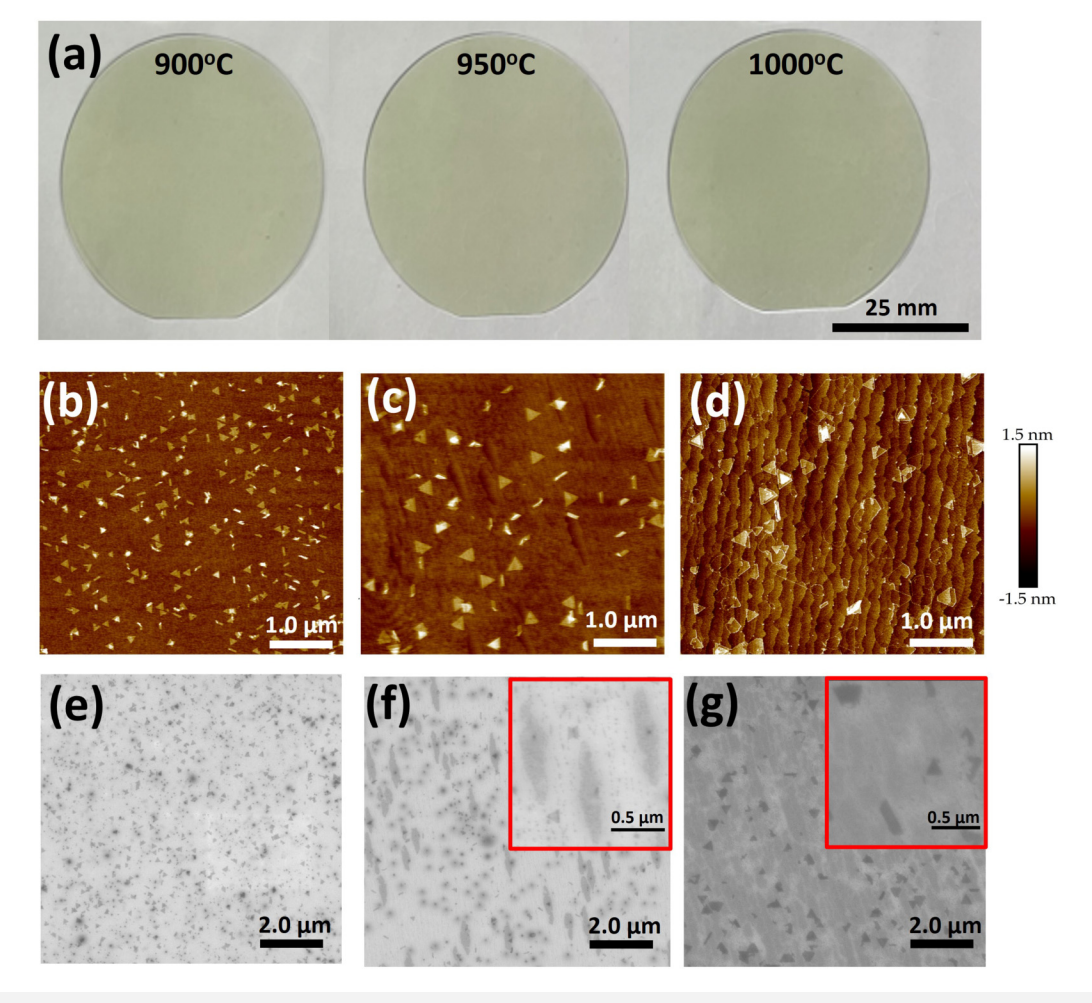


FIG. 1. Surface morphology of MoS_2 monolayer samples. (a) Photos of samples grown at 900, 950, and 1000 °C on 2" c-plane sapphire. AFM images (from the center of wafer) of the MoS_2 monolayers grown at (b) 900, (c) 950, and (d) 1000 °C. FESEM images (from the center of wafer) of the MoS_2 monolayers grown at (e) 900, (f) 950, and (g) 1000 °C.

the MoS_2 at the edge of the 2'' wafer attesting to the good film uniformity [Fig. S2]. The surface of the MoS_2 grown at $1000\,^{\circ}\text{C}$ [Fig. 1(d)] exhibits clearly defined steps that arise from the miscut of the underlying sapphire substrate, which are not as apparent at the lower growth temperatures. FESEM images at the center [Figs. 1(e)–1(g)] and edge of the sample [Figs. S3(b), S3(d), and S3 (f)]²⁸ reveal similar surface coverages of MoS_2 as the AFM images. Analysis of the FESEM images (Table S1)²⁸ indicates that the surface coverage of bilayers decreases from 13% to 5% as the growth temperature is increased from 900 to $1000\,^{\circ}\text{C}$ and the average size of the bilayers increases from 9.5×10^{-3} to $3.3 \times 10^{-2}\,\text{mm}^2$ due to the enhanced diffusivity of precursor adatoms on the monolayer surface at higher temperature. In terms of nucleation and growth of a bilayer on top of the monolayer MoS_2 , the precursor adsorption on the monolayer surface will be substantially reduced and surface diffusion lengths will be

substantially increased compared to the sapphire since the monolayer is a van der Waals surface. We hypothesize that bilayers nucleate at defects in the monolayer; hence, the decrease in bilayer coverage and the increase in bilayer average size suggest that the defect density in the underlying MoS₂ monolayer is reduced as the growth temperature is raised.

In the FESEM images, the underlying monolayer generally exhibits a bright contrast compared to the darker contrast of the bilayer/multilayer regions. At the 950 °C growth temperature [Fig. 1(f)], however, additional features appear in the monolayer characterized by elongated regions of darker contrast that are aligned with the underlying step terraces [inset in Fig. 1(f)]. These darker features become more prominent as the growth temperature is raised to 1000 °C [Fig. 1(g)]. Similar features have been reported in WS₂ monolayers grown by MOCVD on sapphire and have been attributed to variations in electrical conductivity in the WS₂

associated with increased levels of sulfur (sulfur-rich) and oxygen that may originate from variations in the surface termination of the underlying sapphire. Previous work has shown that the hydroxyl (-OH) groups that initially terminate the sapphire surface react with H₂ in the MOCVD growth ambient at elevated temperature forming H₂O. The loss of -OH results in an Al-terminated surface that may then become passivated by sulfur or hydrogen atoms. Consequently, the regions of darker contrast in the FESEM images of the MoS₂, which increase in number and size with growth temperature, likely arise from changes in the surface termination of the sapphire. These changes in surface termination may impact the nucleation and orientation of the MoS₂ domains as well as the adhesion of the MoS₂ monolayer to the underlying sapphire.

B. Crystal quality and epitaxial orientation

In-plane x-ray diffraction (XRD) measurements¹⁷ were performed to investigate the epitaxial relation of the MoS₂ monolayer to the sapphire substrate and compare the crystallographic properties of the MoS₂ films grown at different growth temperatures. An in-plane 2q-w scan at the ϕ angle where the (11 $\bar{2}$ 0) peak of α -Al₂O₃ was observed [Fig. 2(a)] shows two peaks at 37.7° and 58.5° corresponding to the (11 $\bar{2}$ 0) of α -Al₂O₃ and (11 $\bar{2}$ 0) of MoS₂, respectively. The full-width-at-half-maximum (FWHM) of the (11 $\bar{2}$ 0) MoS₂ peak decreases from 0.5° at 900 °C to 0.2° at 1000 °C [Fig. 2(b)], indicating an improvement in crystal quality at higher growth temperature. In-plane XRD ϕ -scans [Fig. 2(c)] confirm that

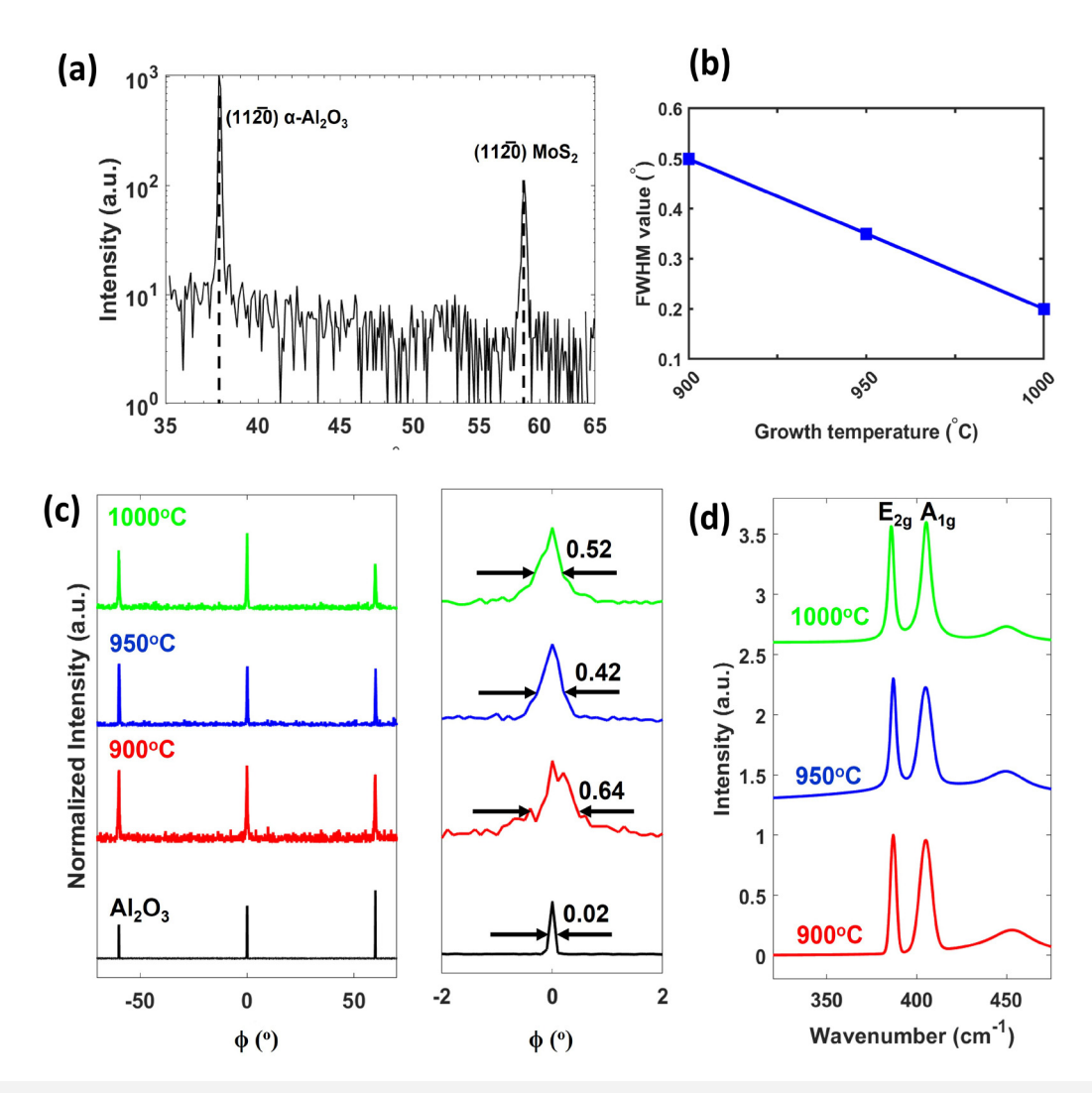


FIG. 2. Crystallographic and vibrational properties of MoS_2 monolayers. (a) In-plane x-ray diffractogram 20 measurement at ϕ = 28.38° showing reflections that correspond to (11 $\overline{2}$ 0) planes of MoS_2 and α -Al₂O₃. (b) FWHM of (11 $\overline{2}$ 0) MoS_2 from 20-scan as a function of growth temperature. (c) In-plane XRD ϕ -scans (left) of MoS_2 as a function of growth temperature confirming the sixfold [11 $\overline{2}$ 0] $MoS_{2(0001)}$ /[11 $\overline{2}$ 0] α -Al₂O₃₍₀₀₀₁₎ epitaxial relationship. The FWHM of the MoS_2 ϕ -scan peak (right) exhibits a minimum at 950 °C. (d) Raman spectra of MoS_2 monolayers as a function of growth temperature.



all the MoS2 films are nominally single crystal and epitaxially oriented with respect to the sapphire. The FWHM of the $\dot{\phi}$ -scan peaks, which provides a measure of the in-plane rotational misorientation of the MoS₂ domains in the monolayer, shows a general decrease with increasing growth temperature [Fig. 2(c)] although the lowest value of 0.42° was obtained for the film grown at 950 °C.

Room-temperature Raman spectra of the MoS₂ monolayers [Fig. 2(d)], fitted by Voight functions [Fig. S5(a)], exhibit in-plane E_{2g}^1 (385.9 cm⁻¹), out-of-plane A_{1g} (405.3 cm⁻¹), and second-order nonresonant 2LA(M) (450 cm⁻¹) Raman active vibrational modes. The Raman frequency difference between the E_{2g}^1 and A_{1g} modes is $< 20~{\rm cm}^{-1}$ (Table S2) 28 for all of the MoS $_2$ samples confirming that the films are monolayer. 18 Raman maps of the MoS₂ grown at 950 and 1000 °C [Fig. S5(b)]²⁸ provide an average FWHM of the A_{1g} modes of 9 ± 4 and 6 ± 2 cm⁻¹, respectively, indicating a reduced number of defects 19 as the growth temperature increases up to 1000 °C, which is consistent with the observed reduction in XRD FWHM [Figs. 2(b) and 2(c)].

C. Microstructure of MoS₂ monolayers

Transmission electron microscopy (TEM) characterization was employed to characterize the microstructure of the MoS₂ monolayers after removal from the sapphire growth substrates and transfer to TEM grids. Selected area diffraction patterns (SAED) obtained along the [0001] zone axis of MoS2 and representative dark-field (DF) TEM micrographs corresponding to the (1010) diffraction spot for samples grown at 900, 950, and 1000 °C are shown in Figs. 3(a)-3(c), respectively. The SAED pattern is consistent with a single crystalline structure for all three MoS₂ monolayers, although as shown in the insets in Figs. 3(a)-3(c), additional spots are present in the SAED patterns for the 950 and 1000 °C samples as will be discussed below. The DF-TEM images reveal regions of bright contrast (white) associated with bilayers/multilayers as well as some wrinkles, tears (black), and folds arising from the transfer process. Within the continuous MoS2 monolayer, regions with differing contrast can be discerned. Regions of medium contrast, such as those outlined in green, are associated with domains bounded by low-angle grain boundaries such as mirror twins (also referred to as inversion domains) and translational line defects. 12,13 Regions of darker contrast within the monolayer, such as those outlined in red, are associated with high-angle grain boundaries. The MoS₂ grown at 900 °C [Fig. 3(a)] contains a substantial fraction (~50% areal coverage) of regions bound by low-angle boundaries with a smaller percentage (~2%) of high-angle grain boundaries. The areal coverage of low-angle grain boundaries within the monolayer is substantially reduced as the growth temperature is increased to ~20% at 950 °C and ~5% at 1000 °C [Fig. S6].²⁸ However, the regions defined by high-angle grain boundaries increase with temperature, from ~2% at 900 °C to ~5% at 950 °C to ~10% at 1000 °C. It is interesting to note that the elongated regions of darker contrast present in the FESEM images of Figs. 1(f) and 1(g) are not apparent in the DF-TEM images of these same samples [Figs. 3(b) and 3(c)], indicating that the FESEM features do not correlate with the grain structure of the MoS2 but instead arise from variations in the interactions/adhesion of MoS2 to the underlying sapphire.

The high-angle grain boundaries observed in the MoS₂ grown at 950 and 1000 °C explain the additional diffraction spots present in the SAED patterns shown in the insets of Figs. 3(a)-3(c). The low-angle grain boundaries in the MoS₂ grown at 900 °C are likely to be mirror-twins, which would be indistinguishable in the SAED pattern. The SAED pattern for the MoS₂ grown at 950 °C [inset in Fig. 3(b)], however, contains an additional diffraction spot of lower intensity adjacent to the main diffraction spot. The SAED pattern for the MoS₂ grown at 1000 °C [inset in Fig. 3(c)] contains multiple distinct low intensity diffraction spots, indicating that the highangle grain boundaries exhibit a wider range of orientations.

To provide a more detailed examination of the domains delineated by both low- and high-angle grain boundaries as well as in-plane strain, we conducted 4D-STEM characterization for the MoS₂ grown at 950 °C. The results are illustrated in Fig. 4 obtained from five distinct regions of the sample. Figure 4(a) displays the virtual HAADF image where white color contrasts denote bilayer/ multilayer regions, gray contrasts represent monolayer MoS2, and black contrasts indicate holes, voids, or wrinkles. This observation parallels the findings in Figs. 1(b)-1(d) and 3. Notably, there is an absence of contrast related to strain and in-plane rotation in the HAADF images. Strain in MoS₂ plays a pivotal role in its physical and electronic properties, influencing its overall performance in various applications.^{20,21} Figures 4(b)-4(d) present the in-plane strain mappings, revealing that a majority of the regions exhibit strain variations below 1%, with the exception of wrinkle zones that arise during the transfer of the sample to a TEM grid. Figure 4(e) delineates the mapping of in-plane grain rotation, distinctly highlighting domains demarcated by grain boundaries. The histogram of these misorientations is showcased in Fig. 4(f), consistently ranging from -5° to 2.5° across all five regions. A positive sign because clockwise rotation, while a negative implies counterclockwise rotation. The average spread of these rotations approximates 2°-3°. By overlaying the two maps of Figs. 4(b) and 4(e), it is found $\overset{\omega}{\approx}$ that the clockwise rotation domains [the orange color with positive degree of rotation in Fig. 4(e)] appear to correspond to the regions with tensile strain [the orange color with tensile strain in Fig. 4(b)] and counterclockwise rotation domains appear to correspond to the regions with compressive strain [the blue color with compressive strain in Fig. 4(b)]. Finally, Fig. 4(g) displays the mapping of the inversion domains. Interestingly, some inversion domains coincide with the domains demarcated by misoriented regions as depicted in Fig. 4(e). This suggests that the inversion domains undergo some degree of rotation, implying that their orientation does not consistently maintain a 60° angle relative to the matrix.

D. Optical properties

Room-temperature photoluminescence (PL) spectra of the MoS₂ monolayers grown at different temperatures are shown in Fig. 5(a). MoS₂ grown at 1000 °C exhibits intense PL emission centered at 1.93 eV and has a higher PL intensity (factor of 2-4) compared to the samples grown at 950 and 900 °C. Given the fact that these samples have comparable bilayer coverage, the higher PL intensity of the MoS2 monolayer grown at 1000 °C could tentatively be attributed to a higher A exciton recombination lifetime and reduced nonradiative recombination.²² Alternatively, the higher PL



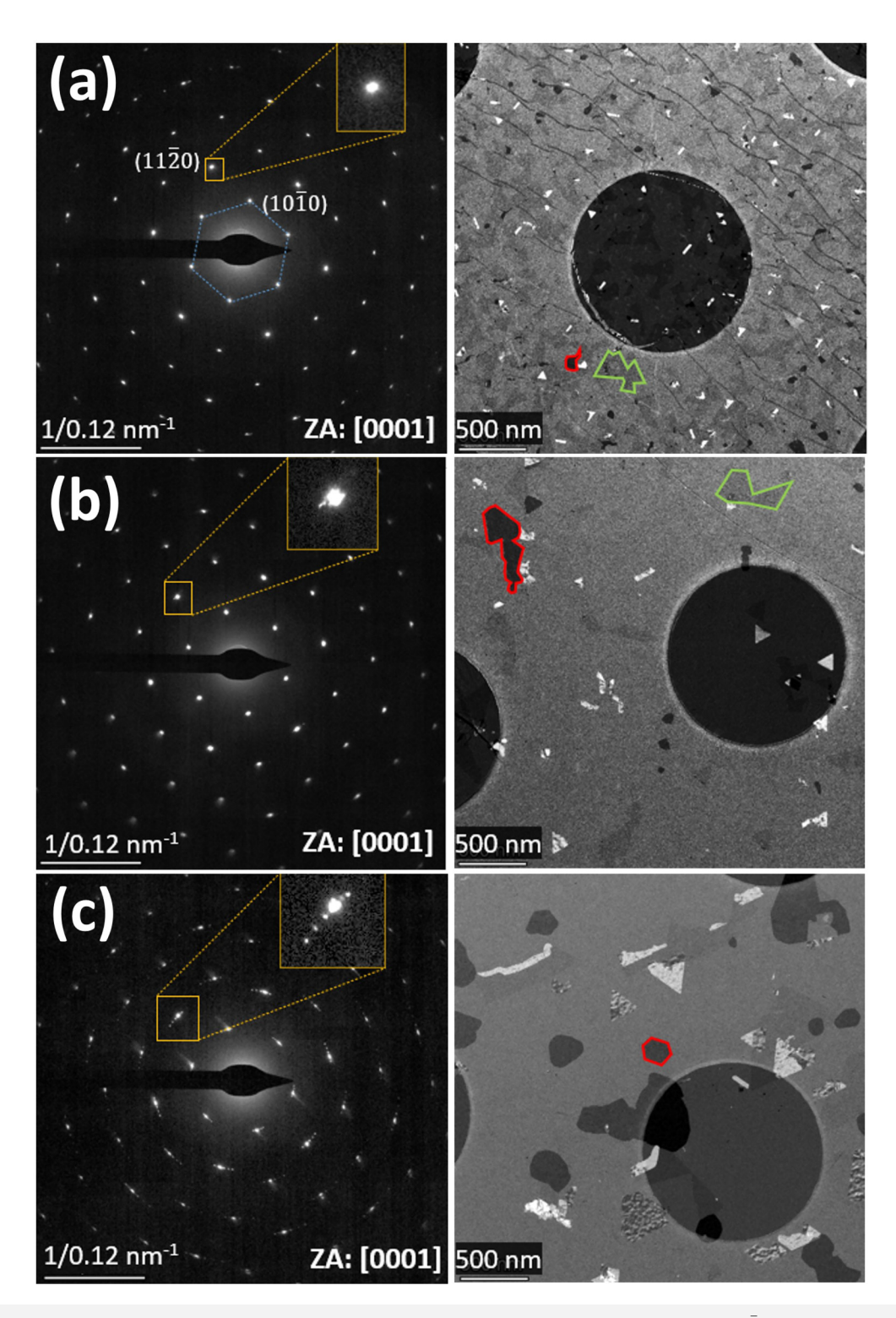


FIG. 3. TEM characterization of MoS_2 monolayers grown at different temperatures. SAED patterns (left) with magnified view of ($11\overline{2}0$) diffraction spot (inset) and DF-TEM micrographs (right) corresponding to the ($10\overline{1}0$) diffraction spot for MoS_2 monolayers grown at (a) 900, (b) 950, and (c) 1000 °C.

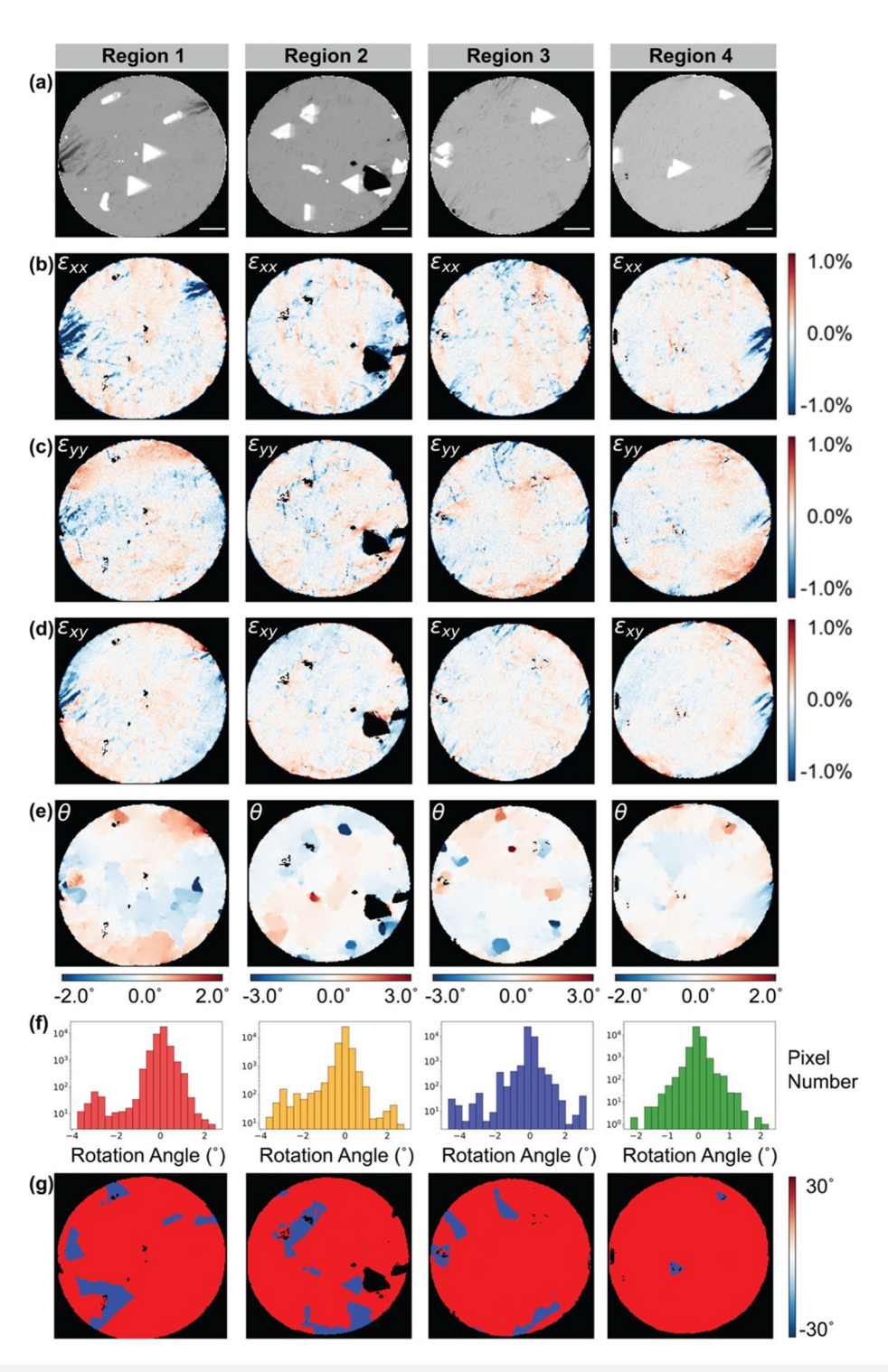


FIG. 4. Comprehensive 4D-STEM imaging and results from four distinct regions of the MoS₂ sample grown at 950 °C. (a) Virtual HAADF images showcasing bilayer/multi-layer regions (white), monolayer MoS₂ (gray), and areas of holes, voids, or wrinkles (black). All scale bars equal to 200 nm. (b)–(d) In-plane strain mappings. (e) Mapping of in-plane grain rotation with clear demarcation of domains by grain boundaries. (f) Histogram representation of misorientations. Positive values indicate clockwise rotations, while negative values depict counterclockwise rotations. (g) Mapping of inversion domain boundaries within the MoS₂ monolayers.

MoS₂ and the sapphire substrate as suggested by the FESEM images [Figs. 1(e) and 1(f)]. To gain a better understanding of the effect of growth temperature on the optical properties, the PL spectra were fit using Voigt functions to identify the contributions of trions (A⁻), neutral excitons (A⁰), and B excitons. A significant blue shift of ~90 meV in the A exciton peak position was observed as the growth temperature increased from 900 to 1000 °C [Fig. 5(b)]. This blue shift could be due to an increase in strain, ~2% estimated compressive strain,²³ induced in the MoS₂ film from growth at high temperature and cooling to room temperature, which arises from differences in the thermal expansion coefficients of MoS₂ $(\alpha_a = 1.9 \times 10^{-6} / ^{\circ}\text{C})^{24}$ and the sapphire $(\alpha_a = 8.1 \times 10^{-6})^{\circ}$ C). To determine the source of the strain and its impact on the PL spectra, the MoS2 monolayer grown at 1000 °C was transferred off of the sapphire growth substrate onto a pristine sapphire substrate. Then, PL characterization was repeated after transfer, as shown in Fig. S7.²⁸ The A exciton position, corresponding to the maximum PL peak position, redshifted after transfer from 1.93 to 1.84 eV, a similar value to that obtained in the MoS₂ on sapphire grown at 900 °C. These results indicate that MoS2 is more strongly coupled to the sapphire at 1000 °C, resulting in significant compressive strain due to thermal expansion mismatch that is

intensity could be associated with differences in the interactions of

released upon layer transfer. The integral ratio of $(A^0 + A^-)/B$ excitons was found to increase with increasing growth temperature, as shown in Fig. 5(c), indicating an improvement in the crystal quality of the MoS₂ monolayers, ²² which is consistent with the results from in-plane XRD and TEM. Spatially resolved PL maps of the integrated PL intensity and peak width (FWHM) (Fig. S8)²⁸ demonstrate that the sample grown at 1000 °C has a more homogeneous distribution and narrower peak FWHM of 20.8 ± 1.7 vs 23.5 ± 4.6 nm for the sample grown at 950 °C. On the other hand, it is interesting to note that the intensity ratio of A⁻/A⁰, which provides a relative measure of trion emission, which is related to the n-type doping level in the film,²⁶ was highest for the MoS₂ grown at 950 °C [Fig. 5(d)]. Background n-type doping in MoS₂ is commonly attributed to sulfur vacancies in the film. The sulfur vacancy concentration would generally be expected to increase as the growth temperature is raised; however, it will also depend on the chemical potential of sulfur in the growth ambient, which could increase with temperature due to an enhanced cracking efficiency of H2S.

E. Electrical transport properties of MoS₂ monolayers

The transport properties of the MoS_2 monolayers grown at different temperatures were characterized using field-effect

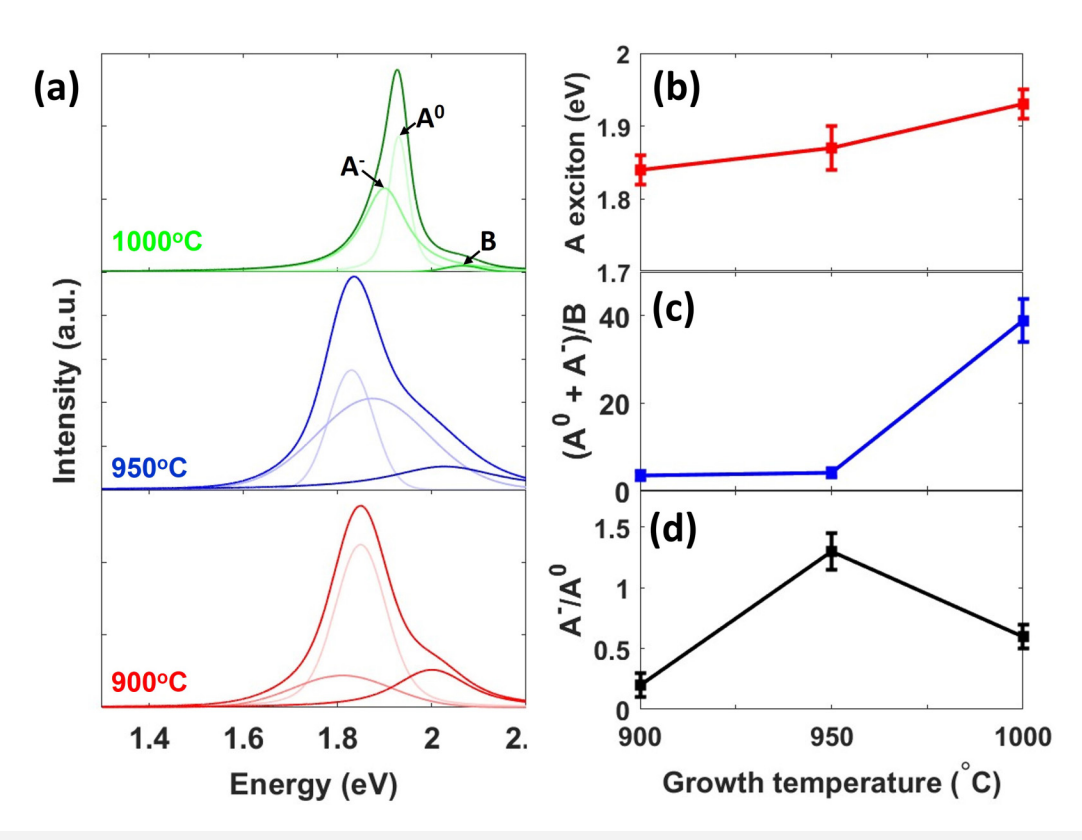


FIG. 5. (a) Room-temperature photoluminescence spectra of MoS_2 monolayer on sapphire grown at 900, 950, and 1000 °C, including the Voigt fitting indicating contributions of trions (A $^-$), neutral excitons (A 0), and B excitons. The dependence of (b) A excitons peak position (c) integral ratio of (A 0 + A $^-$)/B, and (d) intensity ratio of A $^-$ /A 0 on the MoS_2 growth temperature.

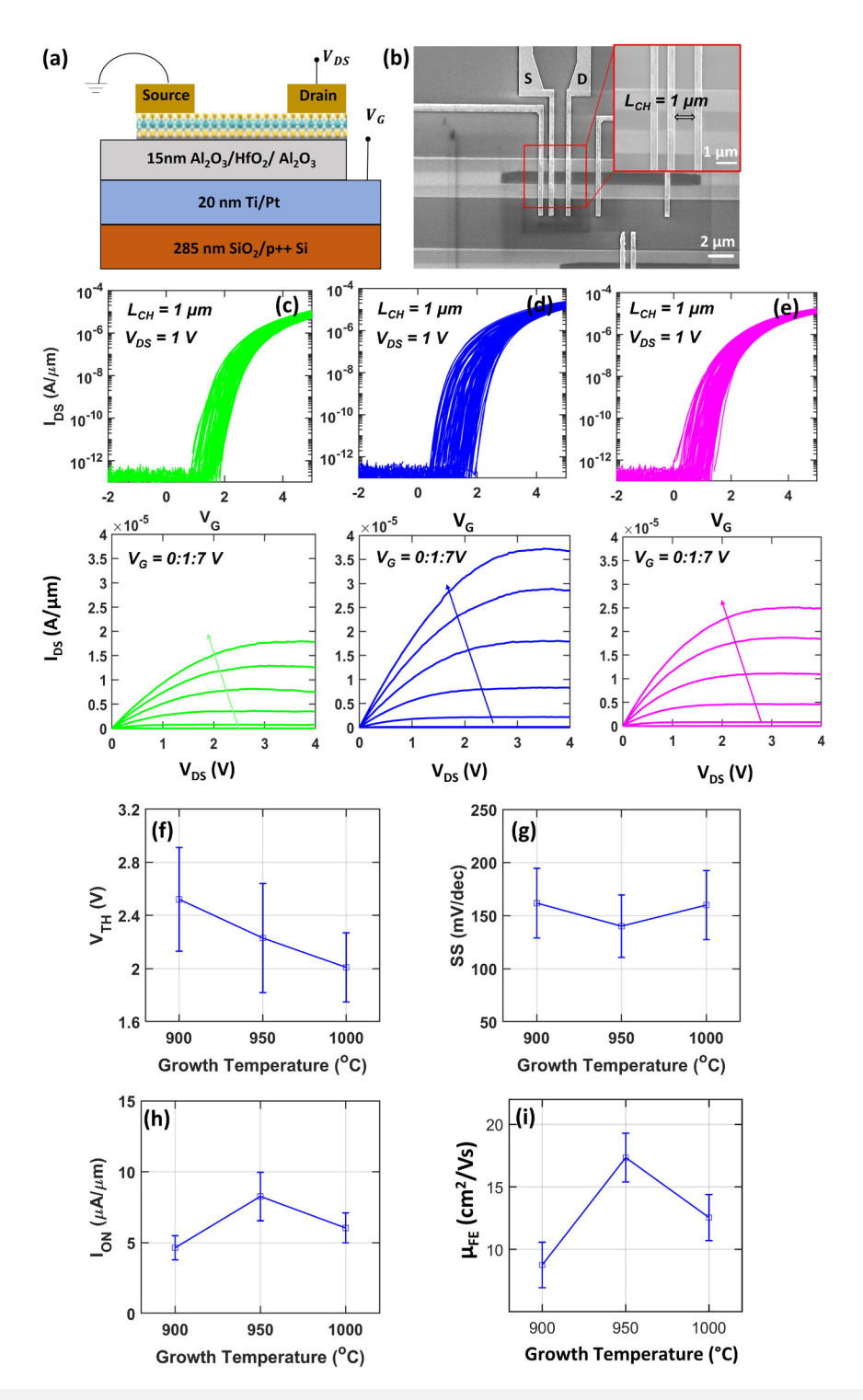


FIG. 6. Electrical transport properties of the MoS_2 monolayers grown at different temperatures. (a) Schematic of back-gated FET device structure. (b) Top-down SEM image of the MoS_2 2D-FET device with L_{CH} = 1 μ m, (c)–(e) (top) transfer characteristics ($I_{DS^*}V_{GS}$) and (bottom) typical output characteristics ($I_{DS^*}V_{DS}$) of the MoS_2 FET devices (~100 devices each) for growth temperatures of (c) 900, (d) 950, and (e) 1000 °C. The dependence of electrical transport properties on the growth temperature of the MoS_2 monolayer FET devices: (f) V_{th} , (g) SS, (h) I_{ON} , and (i) μ_{FE} .



measurements. The FETs were fabricated on 285 nm SiO₂/p⁺⁺-Si substrates with 5 nm Ti/15 nm Pt serving as the local back gate electrodes [Figs. 6(a) and 6(b)]. Additionally, a gate dielectric stack of 9 nm Al₂O₃/3 nm HfO₂/3 nm Al₂O₃ was employed. This gate stack was employed instead of more traditional SiO2 or Si3N4 as it provides a higher dielectric constant enabling a smaller equivalent oxide thickness (EOT), which is crucial for scaling down transistor dimensions in advanced semiconductor technologies.²⁷ The monolayer MoS2 was then transferred to these substrates using the PMMA-assisted wet transfer method, and 20 nm Au/30 nm Ni/20 nm Au metals were utilized as the source and drain contacts. All devices featured a 1 μ m channel length (L_{CH}) and width (W_{CH}), respectively, with the exception of 950 °C where varying channel lengths from 0.5 to $5.0\,\mu\mathrm{m}$ were investigated. Detailed information on the device fabrication can be found in the supplementary information section.²⁸ The transfer characteristics, i.e., the drain-to-source current (I_{DS}), while sweeping the back-gate voltage (V_G) at a constant drain voltage (V_{DS}) of 1 V were measured for 100 devices for each growth temperature of 900, 950, and 1000 °C, as shown in Figs. 5(c)-5(e), respectively. The devices were measured in ambient conditions, and minimal hysteresis was observed for the three samples, as shown in Fig. S9.²⁸ Minimal device-to-device variation (range: ±13%) was observed across all samples, which was attributed to the uniform and contaminant-free MOCVD growth of monolayer TMDs and the clean device fabrication process. Transfer characteristics indicate n-type enhancement mode FETs with normal-off state. Representative output characteristics (IDS-VDS) for each of the devices are also included in Figs. 6(c)–6(e). To further compare the performance of the devices, off-state parameters such as threshold voltage (V_{TH}) and subthreshold slope (SS), along with on-state parameters like peak field-effect mobility (μ_{FE}) and on-current (I_{ON}) at the inversion carrier concentration, were determined for all 100 devices at each growth temperature, and the mean values and standard deviation are depicted in Figs. 6(f)-6(i). The threshold voltage (V_{TH}) was extracted at 100 nA/\mu iso-current and was found to decrease with increasing growth temperature. For instance, the mean V_{TH} reduced from 2.52 ± 0.39 V for MoS₂ grown at 900 °C to $2.01 \pm 0.26 \text{ V}$ for MoS₂ grown at 1000 °C. The decrease in V_{TH} indicates an increase in n-type doping with higher growth temperatures. Furthermore, we extracted the subthreshold slope (SS) of the FETs for two orders of change in the I_{DS} and found that the mean values remained around 160 mV/dec for MoS2 grown at 900 and 1000 °C, while the 950 °C sample showed a reduced mean SS value of 140.05 mV/dec. Field-effect mobility (μ_{FE}), a critical on-state parameter that influences device performance, was extracted using the peak transconductance (μ_{gm}) method. Our results showed a nonmonotonic trend, with mean μ_{FE} increasing from 8.76 cm²/V s for 900 °C MoS₂ to 17.34 cm²/V s for 950 °C MoS₂, and then decreasing to 12.54 cm²/V s for 1000 °C MoS₂. Although threshold voltage indicated higher n-doping with increasing growth temperature, the subthreshold slope and mobility values suggested that while the device performance improved from 900 to 950 °C, a further increase in growth temperature to 1000 °C resulted in performance degradation. This trend is further supported by the mean on-currents (I_{ON}) at an inversion carrier concentration (n_S) of \sim 7.4 × 10¹² cm⁻². Inversion carrier in the channel can be obtained using the following equation:

$$n_s = \frac{C_{ox}(V_G - V_{TH})}{q}.$$

Here, $C_{\rm OX} \approx 5.9 \times 10^{-3} \, \text{F/m}^2$ is the oxide gate capacitance. An approximately $2\times$ increase in mean I_{ON} was obtained when the growth temperature increased from 900 to 950 °C, with the highest mean I_{ON} obtained for the 950 °C growth temperature at $8.27\,\mu\text{A}/\mu\text{m}.$ In contrast, the mean I_{ON} decreased to $6.05\,\mu\text{A}/\mu\text{m}$ for the 1000 °C growth temperature. It should be noted that for TMD FETs, I_{ON} typically decreases and μ_{FE} increases as the L_{CH} is increased as shown in Fig. S10²⁸ for devices fabricated using the 950 °C MoS₂ sample. In general, channel resistance associated with the MoS₂ tends to dominate μ_{FE} for long channel devices while contact resistance (Rc) becomes the dominating factor in the short channel limit (see supplementary information).²⁸ For champion devices fabricated using the 950 °C MoS₂, μ_{FE} ranges from $\sim 25 \text{ cm}^2/\text{V s for } L_{CH} = 0.5 \text{ mm to } \sim 32 \text{ cm}^2/\text{V s for } L_{CH} = 5.0 \text{ mm}.$

Overall, the electrical results indicate that a high density of low-angle grain boundaries (most prevalent in MoS2 grown at 900 °C) have a negative impact on FET performance likely due to a reduction in field-effect mobility. However, point defects, e.g., sulfur vacancies as well as high-angle grain boundaries, also play a role in degrading FET performance, as observed in the MoS₂ grown at 1000 °C sample.

IV. SUMMARY AND CONCLUSIONS

The effects of growth temperature on the structural, optical, and transport properties of epitaxial MoS₂ monolayers grown on 2" c-plane sapphire by MOCVD were investigated. Overall, a general & improvement in the crystalline properties of the MoS₂ monolayers was observed as the growth temperature was increased from 900 to $\overset{\omega}{\bowtie}$ 1000 °C as evidenced by a reduction in the FWHM of the (11 $\bar{2}$ 0) MoS₂ peak from in-plane XRD 2q-w scans, a significantly reduced density of low-angle grain boundary defects from DF-TEM, an increased A-exciton intensity and decreased A-exciton FWHM from room temperature PL and a reduced FWHM of the MoS $_2$ A $_{1\mathrm{g}}$ peak in the Raman spectra. The presence of a high number of lowangle grain boundaries observed in DF-TEM clearly impacts the FET performance, leading to a markedly reduced I_{ON} and μ_{FE} for devices fabricated using the 900 °C MoS2 compared to devices fabricated using the 950 and 1000 °C epilayers (Table S3).²⁸ For the 900 °C MoS₂ sample, the grains that are bounded by low-angle boundaries are on the order of 50-200 nm in size; hence, a FET with $L_{CH} = 1 \,\mu\text{m}$ will include several of these low-angle grain boundaries within the channel region. Consequently, it is important to minimize low-angle grain boundaries in epitaxial TMD monolayers to optimize FET performance.

It is nevertheless interesting that the highest I_{ON} and μ_{FE} were obtained for devices fabricated with the 950 °C MoS₂ rather than the 1000 °C MoS₂, which from 2q-w XRD, Raman and PL would appear to have the highest crystal quality. The SAED patterns and DF-TEM images reveal that the areal percentage of high-angle grain boundaries increases from 2% at 900 °C to 10% at 1000 °C. While a 10% areal coverage in the 1000 °C sample would appear to



be relatively small, the highly misoriented domains are well distributed throughout the MoS₂ monolayer as evident in Fig. 3, exhibiting grain sizes in the range of 50-200 nm. Consequently, many of the FETs with $L_{CH} = 1 \,\mu\text{m}$ will include at least one of these highangle grain boundaries within the channel region, which could negatively impact device performance.

The changes in the type and density of low-angle and highangle grain boundaries observed in the MoS2 monolayers with growth temperature are intimately tied to the density and orientation of nuclei on the sapphire surface. While the nucleation process was not investigated in detail in this study, it is clear from the AFM and FESEM images included in Fig. 1 that the underlying sapphire is changing as the growth temperature is increased as the steps become more pronounced in AFM and the regions of darker contrast in FESEM, attributed to changes in adhesion of the MoS2 to sapphire, increase in number and size. This is undoubtably related to changes in surface termination of the sapphire, which impact the nucleation and orientation of the MoS2 domains and the inhomogeneity in the in-plane strain. The results clearly illustrate that inversion domains are reduced by increasing the growth temperature, but there is a trade-off as more highly misoriented domains also start to appear. We speculate that as the growth temperature is increased from 900 to 950 °C, the sapphire surface becomes more Al-terminated and this is an important factor that is responsible for a reduction in mirror twins. However, as the growth temperature is increased further to 1000 °C, the steps on the sapphire are modified via step-bunching or a related mechanism that causes nucleation of highly misoriented domains. Further studies are needed to investigate this in detail.

The results demonstrate that the use of 2q-w XRD, Raman, and PL cannot be reliably used as figures of merit to optimize MoS₂ epilayers for high-performance FET devices. Detailed investigation of the microstructure of the monolayer is required in order identify the presence of both low-angle and high-angle grain boundaries that may impact device performance. Interestingly, the FWHM of the in-plane XRD ϕ -scan peak, which provides a measure of the rotational misorientation of MoS2 domains within the monolayer, appears to correlate best with FET performance although further studies are needed to verify this metric. It should be noted that this study has focused exclusively on line defects in MoS₂ epitaxial monolayers while point defects such as sulfur vacancies will also play an important role in FET performance.

ACKNOWLEDGMENTS

The authors acknowledge the primary financial support of the National Science Foundation (NSF) through the 2D Crystal Consortium-Materials Innovation Platform (2DCC-MIP) under NSF Cooperative Agreement No. NSF DMR-2039351. N. Trainor acknowledges the National Science Foundation Graduate Research Fellowship Program under Grant No. DGE1255832H. Myja, T. Kümmell and G. Bacher received funding from the German Research Foundation (DFG) under the Project No. BA 1422/21-1. Y. Zhang, A. Bisht, and N. Alem acknowledge the NSF CAREER Grant No. 500000003802 for TEM characterization. D. A. Kowalczyk acknowledges the financial support from the National Science Centre, Poland (No. 2018/30/E/ST5/00667) and the

Fulbright Junior Research Award granted by the Polish-U.S. Fulbright Commission. M. E. Leger acknowledges support from National Aeronautics and Space Administration, NASA Grant No. 80NSSC19M0201. T. V. Mc Knight acknowledges support from the U.S. Air Office of Scientific Research and Clarkson Aerospace Corp. under Award No. FA9550-21-1-0460.

AUTHOR DECLARATIONS

Conflict of Interest

The authors have no conflicts to disclose.

Author Contributions

Chen Chen: Writing - original draft (equal). Nicholas Trainor: Data curation (supporting); Investigation (supporting); Methodology (supporting); Writing - review & editing (supporting). Shalini Kumari: Data curation (supporting); Investigation (supporting); Methodology (supporting); Supervision (supporting); Writing - review & editing (equal). Henrik Myja: Investigation (supporting); Methodology (supporting); Supervision (supporting); Validation (supporting); Writing - review & editing (supporting). Tilmar Kümmell: Data curation (equal); Investigation (equal); Methodology (equal); Writing - review & editing (equal). Zhiyu Zhang: Investigation (supporting); Methodology (supporting); Writing - review & editing (supporting). Yuxi Zhang: Investigation (supporting); Methodology (supporting); Writing review & editing (supporting). Anuj Bisht: Investigation (supporting); Methodology (supporting); Writing – review & editing (supporting). Muhtasim Ul Karim Sadaf: Data curation (supporting); Formal analysis (supporting); Investigation (supporting); Methodology (supporting); Investigation (supporting); Methodology (supporting); Writing - review & editing (supporting). **Najam U. Sakib:** Formal analysis (supporting); Investigation (supporting); Methodology (supporting); Writing – review & 3 editing (supporting). Ying Han: Investigation (supporting); & Methodology (supporting). Thomas V. Mc Knight: Investigation (supporting). Andrew R. Graves: Data curation (supporting); Investigation (supporting); Methodology (supporting); Writing review & editing (supporting). Meghan E. Leger: Formal analysis (supporting); Investigation (supporting); Methodology (supporting). Nicholas D. Redwing: Investigation (equal); Supervision (equal); Writing - review & editing (equal). Myeongok Kim: Formal analysis (supporting); Investigation (supporting); Methodology (supporting); Writing – review & editing (supporting). **Dorota Anna Kowalczyk:** Investigation (supporting); Methodology (supporting); Writing - review & editing (supporting). Gerd Bacher: Writing - review & editing (supporting). Nasim Alem: Investigation (supporting). Yang Yang: Investigation (supporting); Methodology (supporting); Writing - review & editing (supporting). Saptarshi Das: Investigation (supporting); Methodology (supporting). Joan M. Redwing: Investigation (equal); Supervision (equal); Writing - review & editing (equal).

DATA AVAILABILITY

The data that support the findings of this study are openly available in ScholarSphere at http://doi.org/10.26207/4ez5-7450, Ref. 29.



REFERENCES

- ¹S. B. Samavedam *et al.*, 2020 IEEE International Electron Devices Meeting (IEDM), San Francisco, CA, 12–18 December 2020 (IEEE, New York, 2020), pp. 1.1.1–1.1.10.
- pp. 1.1.1–1.1.10.

 ²W. Cao, J. Kang, D. Sarkar, W. Liu, and K. Banerjee, IEEE Trans. Electron. Dev. 62, 3459 (2015).
- ³K. Kang, S. Xie, L. Huang, Y. Han, P. Y. Huang, K. F. Mak, C. J. Kim, D. Muller, and J. Park, Nature 520, 656 (2015).
- ⁴J. Zhu et al., Nat. Nanotechnol. 18, 456 (2023).
- ⁵X. Zhang et al., Nano Lett. **18**, 1049 (2018).
- ⁶D. Chiappe et al., Nanotechnology 29, 425602 (2018).
- ⁷M. Marx et al., J. Cryst. Growth **464**, 100 (2017).
- ⁸M. Chubarov et al., ACS Nano 15, 2532 (2021).
- ⁹T. Li et al., Nat. Nanotechnol. 16, 1201 (2021).
- ¹⁰J. Wang et al., Nat. Nanotechnol. 17, 33 (2022).
- ¹¹H. Zhu et al., Nat. Nanotechnol. **18**, 1295 (2023).
- ¹²A. M. Van Der Zande et al., Nat. Mater. **12**, 554 (2013).
- ¹³D. Reifsnyder Hickey et al., Nano Lett. **21**, 6487 (2021).
- ¹⁴W. Zhou et al., Nano Lett. 13, 2615 (2013).
- 15 Y. Xuan et al., J. Cryst. Growth 527, 125247 (2019).
- ¹⁶V. Spampinato, Y. Shi, J. Serron, A. Minj, B. Groven, T. Hantschel, P. van der Heide, and A. Franquet, Adv. Mater. Interfaces 10, 2202016 (2023).
- ¹⁷M. Chubarov, T. H. Choudhury, X. Zhang, and J. M. Redwing, Nanotechnology 29, 055706 (2018).
- ¹⁸C. Lee, H. Yan, L. E. Brus, T. F. Heinz, J. Hone, and S. Ryu, ACS Nano 4, 2695 (2010).

- ¹⁹S. Mignuzzi, A. J. Pollard, N. Bonini, B. Brennan, I. S. Gilmore, M. A. Pimenta, D. Richards, and D. Roy, Phys. Rev. B 91, 195411 (2015).
- ²⁰A. Castellanos-Gomez, R. Roldán, E. Cappelluti, M. Buscema, F. Guinea, H. S. J. Van Der Zant, and G. A. Steele, Nano Lett. 13, 5361 (2013).
- ²¹S. Bhattacharyya, T. Pandey, and A. K. Singh, Nanotechnology 25, 465701 (2014).
- ²²K. M. McCreary, A. T. Hanbicki, S. V. Sivaram, and B. T. Jonker, APL Mater. **6**, 111106 (2018).
- ²³H. J. Conley, B. Wang, J. I. Ziegler, R. F. Haglund, S. T. Pantelides, and K. I. Bolotin, Nano Lett. 13, 3626 (2013).
- ²⁴S. H. El-Mahalawy, B. L. Evans, and J. J. Thomson, J. Appl. Cryst. **9**, 403 (1976).
- **25**W. M. Yim and R. J. Paff, J. Appl. Phys. **45**, 1456 (1974).
- ²⁶S. Mouri, Y. Miyauchi, and K. Matsuda, Nano Lett. 13, 5944 (2013).
- ²⁷S. Das et al., Nat. Eletron. 4, 786 (2021).
- $^{\mathbf{28}}$ See supplementary material online for details of the MoS $_2$ monolayers' synthesis by MOCVD and characterization methods including AFM and FESEM imaging, in-plane XRD, Raman spectrum analysis, TEM imaging, 4D-STEM characterization, PL spectrum and PL mapping result, MoS2 monolayer transfer process and FET device fabrication and electrical characterization method.
- ²⁹C. Chen, N. Trainor, and J. M. Redwing (2023). "Effect of growth temperature on the microstructure and properties of epitaxial MoS2 monolayers grown by metalorganic chemical vapor deposition," Scholarsphere, Dataset http://doi.org/10.26207/4ez5-7450